Antibody Therapeutics, 2023, Vol. 6, No. 1 **1–12**
https://doi.org/10.1093/abt/tbac027
Advance Access Publication on 7 November 2022

Original research article

A novel humanized Chi3l1 blocking antibody attenuates acetaminophen-induced liver injury in mice

Leike Li[1], Yankai Wen[2], Daniel Wrapp[3], Jongmin Jeong[2], Peng Zhao[1], Wei Xiong[1], Constance Lynn Atkins[2], Zhao Shan[2,4], Deng Hui[1], Jason S. McLellan[3], Ningyan Zhang[1,*], Cynthia Ju[2,*] and Zhiqiang An[1,*]

[1]Texas Therapeutics Institute, Brown Foundation Institute of Molecular Medicine, McGovern Medical School, The University of Texas Health Science Center at Houston, Houston, TX 77030, USA , [2]Department of Anesthesiology, McGovern Medical School, The University of Texas Health Science Center at Houston, Houston, TX 77030, USA , [3]Department of Molecular Biosciences, The University of Texas at Austin, Austin, TX 78712, USA , and [4]Center for Life Sciences, School of Life Sciences, Yunnan University, Kunming 650106, China

Received: August 1, 2022; Revised: October 24, 2022; Accepted: October 27, 2022

ABSTRACT

Acetaminophen (APAP) overdose is a leading cause of acute liver injury in the USA. The chitinase 3-like-1 (Chi3l1) protein contributes to APAP-induced liver injury (AILI) by promoting hepatic platelet recruitment. Here, we report the development of a Chi3l1-targeting antibody as a potential therapy for AILI. By immunizing a rabbit successively with the human and mouse Chi3l1 proteins, we isolated cross-reactive monoclonal antibodies (mAbs) from single memory B cells. One of the human and mouse Chi3l1 cross-reactive mAbs was humanized and characterized in both *in vitro* and *in vivo* biophysical and biological assays. X-ray crystallographic analysis of the lead antibody C59 in complex with the human Chi3l1 protein revealed that the kappa light contributes to majority of the antibody–antigen interaction; and that C59 binds to the 4α-5β loop and 4α-helix of Chi3l1, which is a functional epitope and hotspot for the development of Chi3l1 blocking antibodies. We humanized the C59 antibody by complementarity-determining region grafting and kappa chain framework region reverse mutations. The humanized C59 antibody exhibited similar efficacy as the parental rabbit antibody C59 in attenuating AILI *in vivo*. Our findings validate Chi3l1 as a potential drug target for AILI and provide proof of concept of developing Chi3l1 blocking antibody as a therapy for the treatment of AILI.

Statement of Significance: We characterized a chitinase 3-like-1 (Chi3l1)-neutralizing rabbit monoclonal antibody (C59) which attenuates acetaminophen-induced liver injury in mice. X-ray crystallography revealed that kappa light contributes more to the antibody–antigen interaction; and that C59 binds to the 4α-5β loop and 4α-helix of Chi3l1, which is a functional epitope. The humanized antibody retained the functional profile of the parental antibody.

KEYWORDS: Chi3l1; acetaminophen; liver injury; antibody therapy; rabbit antibody; humanized antibody

INTRODUCTION

Acetaminophen (APAP) is a widely used analgesic for relieving pain and reducing fever. It is generally safe at the therapeutic dose. However, APAP overdose causes liver damage, which can lead to acute liver failure [1]. It is estimated that 80,000 patients in the USA are admitted to the emergency room annually due to APAP-induced liver injury (AILI) [2]. AILI contributes to nearly 50% of drug-induced liver injuries in the USA [3]. Although *N*-acetylcysteine (NAC) can prevent the injury, it has a narrow window for therapeutic intervention. The efficacy of NAC dramatically decreases when given more than a few hours

*To whom correspondence should be addressed. Ningyan Zhang, Cynthia Ju, Zhiqiang An. Email: Ningyan.zhang@uth.tmc.edu, Changqing.Ju@uth.tmc.edu, Zhiqiang.an@uth.tmc.edu

after the APAP overdose [4]. Thus, the development of novel therapeutic drugs is urgently needed for the effective and specific treatment of AILI.

APAP is metabolized by cytochrome P450 into the toxic metabolite *N*-acetyl-*p*-benzoquinone imine (NAPQI) in the liver [5]. Excess NAPQI in APAP overdose causes severe mitochondrial dysfunction, hepatocyte necrosis and further drives the liver injury [6]. The severity of AILI is not only determined by the amount of NAPQI but also impacted by the inflammation responses following the injury [7, 8]. As revealed in mouse AILI models and studies in human patients, necrotic hepatocytes release the damage-associated molecular patterns (DAMPs), such as HMGB1 [9], which stimulate the resident hepatic macrophages and neutrophils to secret proinflammatory cytokines, such as TNF-α and IL-1β. These cytokines and immune responses further enhance inflammation and increase the recruitment of monocyte-derived macrophages and neutrophils into the liver [10]. It has been reported that neutralizing the proinflammatory activity of HMGB1 by heparan sulfate octadecasaccharide dramatically attenuates AILI and has a therapeutic advantage over NAC for delayed treatment in a mouse model [11]. Thus, inhibiting the inflammatory events, which involve functional interplays among immune cells, is a viable treatment strategy for AILI.

We have reported previously an increased hepatic platelet accumulation in AILI patients' liver tissue and demonstrated that the secreted protein chitinase 3-like-1 (Chi3l1) drives the platelet recruitment into the mouse liver and promotes acute liver injury [12]. Therefore, blocking the Chi3l1 function by an antibody may have a protective effect against AILI. Chi3l1 belongs to the chitinase protein family, which catalyzes the cleavage of β-1,4-glycosidic bond in the chitin and chitooligosaccharides, which are widely distributed in fungi and the exoskeletons of insects [13]. Although rodents and mammals do not produce chitin, they express active chitinases (CHIT1 and AMCase) [14, 15] as well as chitinase-like proteins (CLPs) lacking the enzymatic activity [16]. Chi3l1 is one of the CLPs in both humans and mice [17, 18]. Chi3l1 adopts the conserved (α/β)8-barrel structure of metabolic enzyme proteins, allowing it to bind to chitin oligosaccharides and other polysaccharides such as heparin sulfate [19, 20]. Chi3l1 is associated with a range of pathologies and is overexpressed under the condition of type 2 activation of immune responses [21], but its function remains poorly understood.

In this study, we describe the isolation and characterization of a blocking monoclonal antibody (mAb) C59, which is cross-reactive to the mouse Chi3l1 (mChi3l1) and human Chi3l1 (hChi3l1) proteins. Antibody C59, which was isolated from a single memory B cell of a rabbit immunized successively with hChi3l1 and mChi3l1 proteins, significantly attenuates AILI in mice. Structural analysis of the Chi3l1 + C59-Fab complex by X-ray crystallography revealed that C59 binds to the 4α-5β loop and 4α-helix of Chi3l1. To develop the antibody as a potential therapy for AILI, we humanized the rabbit antibody, and the humanized C59 (hC59) retains the biophysical and biological properties of the parental antibody *in vitro* and *in vivo*.

MATERIALS AND METHODS

Chi3l1 protein expression

The hChi3l1 (UniProt, #P36222) and mChi3l1 (UniProt, #Q61362) were expressed in Expi293F (Thermo Fisher Scientific) cells with Avitag (GLNDIFEAQKIEW HE) and His tag at the C-terminal of the sequences. The proteins were purified using the Ni-NTA Agarose (Invitrogen) according to the manufacturer's instructions. The biotinylation of Chi3l1 was performed using BirA ligase (Avidity, #BirA500). The hChi3l1 without tags for X-ray crystallography was expressed in Expi293F (Thermo Fisher Scientific) cells and was in-house purified by affinity chromatography using the HiPrep Heparin FF (Cytiva) and by size exclusion chromatography using the HiLoad 16/600 Superdex 200 pg column (Cytiva) according to the manufacturer's instructions.

Rabbit immunization and single rabbit memory B cell culture

Two female New Zealand White rabbits (10–16 weeks of age, Charles River Labs) were injected subcutaneously with 400 μg of hChi3l1 and Complete Freund's Adjuvant (Sigma). The rabbits were boosted with 200 μg of hChi3l1 and incomplete Freund's Adjuvant (Sigma) subcutaneously. To generate anti-mChi3l1 antibodies, the rabbit-#2 was boosted with mChi3l1 (200 μg) and incomplete Freund's Adjuvant (Sigma) subcutaneously.

The peripheral blood mononuclear cells (PBMCs) were isolated from the immunized rabbit by the ACCUSPIN™ system (Sigma). The antigen-specific memory B cells were enriched by biotinylated Chi3l1 and Streptavidin MicroBeads (Miltenyi Biotec) according to the manufactory's instructions. The single memory B cells were seeded into 96-well cell culture plates, at a density of about one cell/per well, with pre-coated EL4-B5 feeder cells (Kerafast). The feeder cells were irradiated with 50 Gy in a gamma radiation chamber before use. The single memory B cells were cultured in 100 μL of RPMI-1640 (10% FBS) with IL-2 (10 U/mL, R&D Systems), IL-21 (10 U/mL, R&D Systems) at 37 °C, 5% CO_2 and 93% humidity for 14 days. The supernatant was collected to detect the antibody concentration and the antigen-binding of the antibodies.

Supernatant antibody concentration measurement

Mouse anti-rabbit IgG antibody (Jackson ImmunoResearch) was coated on the ELISA plate at 4 °C overnight. The plate was washed once with TBST and blocked with 1% (v/v) BSA in TBST for 1 h at room temperature. The plate was incubated with the supernatants for 1 h at room temperature to capture the antibodies from the supernatants. After washing the plates three times with TBST, alkaline phosphatase-conjugated donkey anti-rabbit IgG (Jackson ImmunoResearch) was added at the dilution of 1:5,000 in TBST for 1 h. After washing three times with TBST again, the plates were incubated with 100 μL/well of 4-methylumbelliferyl phosphate (Sigma), for 15–60 minutes at room temperature. The fluorescence

signal was measured with excitation at 360 nm and emission at 440 nm. The standard binding curve of the control rabbit antibody was included to calculate the supernatant antibody concentration using GraphPad Prism 8.

Positive supernatant antibody screening

The ELISA binding assay was performed with a previously reported protocol with modifications [22]. Briefly, purified hChi3l1 or mChi3l1 proteins were coated at 2 μg/mL in PBS on 96-well microtiter plates (Corning) at 4 °C overnight. The plates were washed once with PBST and then blocked with 1% (v/v) BSA in PBST for 1 hour. The supernatants were diluted at 1:20 dilution in PBST and then incubated with the antigen-coated plates for 1.5 hours. After incubation and washing, the HRP-conjugated goat Anti-Rabbit IgG F(ab')2 (Jackson ImmunoResearch) was added at the dilution of 1:5,000 in PBST for 1 hour. After washing three times with PBST, the plates were then incubated with 100 μL/well of the tetramethylbenzidine substrate (Thermo Fisher Scientific) for 3–5 minutes at room temperature. The reaction was stopped by 50 μL/well of 1 M H_2SO_4, and the absorbance was measured at 450 nm on a microplate reader (Molecular Devices).

Antibody cloning and humanization

Antibody cloning from positive single memory B cells was performed with a previously reported protocol with modifications [23]. Briefly, total RNA from the cells in the positive wells was isolated using RNeasy Micro Kit (Qiagen) and was converted to cDNA using iScript™ cDNA Synthesis Kit (Bio-Rad). The IgG genes were recovered based on the reported methods [24]. Recombinant antibodies were expressed by transient transfection in Expi293F cells and purified by protein A affinity chromatography.

Humanization of the Chi3l1 antibody was performed by complementarity determining regions (CDR)-grafting as described previously with modifications [25, 26]. Briefly, CDRs of the rabbit antibody were defined by Kabat numbering system. The most closely related human germline sequence were identified by blasting with the parental rabbit mAb in the IMGT database. Then, the rabbit CDRs were grafted into the most closed human antibody germline. The residues in the frame region which are known to be structurally critical were retained based on previous publications [25, 26]. The humanized DNA fragments were synthesized (GenScript) and then cloned into human IgG1/IgK vectors. The site-specific mutagenesis in the kappa chain was generated by overlap extension PCR using primer with single amino acid mutations.

Antibody–antigen affinity measurement and epitope binning

The antibody affinity was measured by Bio-Layer Interferometry using the Octet RED96 (FortéBio). The antibodies were diluted to 200 nM in PBST and were loaded onto the protein A biosensors for 5 minutes. The coated biosensors were incubated with a series of recombinant Chi3l1 concentrations (0–200 nM) for 3 minutes and were then washed in PBS for another 2 minutes for dissociation. The ForteBio's data analysis software was used to fit the binding curve to a 1:1 binding model to extract an association rate and dissociation rate. The affinity (K_D) was calculated using the ratio koff/kon.

The epitope binning was performed in an Octet RED96 system to demonstrate if two antibodies bind to the overlapped epitope. Briefly, the first antibody (200 nM) was incubated with the protein A biosensors for 5 minutes. Then, the remaining Fc-binding sites on the biosensors were blocked with an irrelevant rabbit antibody (400 nM) for 5 minutes. Following a 1-minute wash in PBST, the biosensors were then incubated with the recombinant Chi3l1 (200 nM) for 5 minutes to saturate the binding site of the first antibody. Finally, the biosensors were incubated with the secondary antibodies (200 nM) for 5 minutes. The signal was recorded for binding of the secondary antibodies to Chi3l1. If no signal increases, the two antibodies were classified in the same epitope bin (competitor, overlapped epitope). By contrast, if an increased binding signal was observed with the second antibody, the two antibodies were classified in different epitope bins (non-competitor). Raw data were processed using ForteBio's data analysis software 11.0.

X-ray crystallographic studies

The C59 Fab was prepared using Immobilized Papain (Thermo Fisher Scientific) according to the manufactory's instruction. An excess of hChi3l1 protein was mixed with purified C59 Fab and was incubated at 4° for roughly 1 hour to allow binding to occur. The mixture was then loaded onto a Superdex 200 Increase 10/300 GL column in 2 mM Tris pH 8.0, 200 mM NaCl and 0.02% NaN_3 to purify the Chi3l1 + Fab complex from excess unbound Chi3l1. Peak fractions corresponding to the complex were collected and concentrated to 7.00 mg/mL for crystallization. Chi3l1 + C59 Fab complex crystals were grown by vapor diffusion in sitting drops in a mother liquor composed of 2 M sodium formate and 0.1 M sodium acetate pH 4.6. X-ray diffraction data were collected at the Advanced Light Source beamline 5.0.1 and were indexed, integrated and scaled with iMOSFLM and AIMLESS [27, 28]. The complex structure was solved by molecular replacement using Phaser MR and ensembles derived from PDB entries 4P8V, 6PEH and 4BHC. Model building and refinement were performed using Coot, Phenix and ISOLDE [29–31].

Efficacy evaluation of the anti-Chi3l1 mAbs *in vivo*

For APAP treatments, C57BL/6J male mice (8–12 weeks of age, 3-6 mice/group) were fasted overnight (5:00 pm–9:00 am) before intraperitoneally (i.p.) injected with APAP (Sigma, A7085) at a dose of 210 mg/kg. To examine the therapeutic potential of Chi3l1 mAbs, the mice were injected (i.p.) with either a control antibody or anti-Chi3l1 antibody (5 μg/mouse in 100 μL of PBS) 3 hours after APAP administration. Liver paraffin sections and sera were harvested at time points indicated in the figure legends. Serum alanine transaminase (ALT) levels were measured

using a diagnostic assay kit (Teco Diagnostics). Student's *t*-test was performed.

Statistics

Statistical analyses were carried out using GraphPad Prism (GraphPad Software). Comparisons between two groups were carried out using unpaired Student's *t*-test. The *p*-values were labeled and <0.05 was considered to be significantly different statistically.

RESULTS

Development of rabbit mAbs targeting Chi3l1

We first developed a method for isolating rabbit mAbs by single memory B cell culturing and cloning (Fig. 1A and B). Briefly, after the rabbits were immunized with the hChi3l1 protein (Rabbit-#1 and Rabbit-#2), the serum titer was detected before the B cell isolation and culture. Both rabbits' sera bind to hChi3l1 at 10^{-6} dilution, but relatively lower binding titer to mChi3l1 (10^{-5} dilution) (Fig. 1C). We then isolated the hChi3l1-specific memory B cells by antigen baiting, which involves the use of biotinylated hChi3l1 (through an Avitag) and streptavidin magnetic beads. The enriched memory B cells were then grown in single-cell culture with the supplement of EL4-B5 feeder cell and the cytokine cocktail of rabbit IL-2 and IL-21. After 2 weeks of culturing, 15.7% of the single B cells (31/197) expressed and secreted antibodies at an average concentration of 48.3 ng/mL (Fig. 1D). Of the 31 single B cells that expressed antibodies, 24 bound to hChi3l1 as determined by ELISA using B cell supernatants; however, none of them bound to mouse Chi3l1 (Fig. 1E). The genes encoding the heavy and light chain variable regions were cloned from the 24 single memory B cells into a rabbit IgG expression vector. We were able to express 23 of the 24 antibodies in Expi293F cells and purify them by Protein A columns, which represents a 96% antibody gene recovery rate from the positive single memory B cells. To study the efficacy in mice, we need the hChi3l1 antibodies to be cross-reactive to mChi3l1. As observed in the ELISA titer (Fig. 1C), immunization with the hChi3l1 protein elicited cross-reactive antibodies to both hChi3l1 and mChi3l1 proteins. We then isolated mChi3l1-specific individual memory B cells from the rabbit immunized with hChi3l1. After B cell culturing, we tested the binding of the B cell supernatants to both hChi3l1 and mChi3l1. Of the 240 single B cell supernatants, only four exhibited minimal binding to mChi3l1 by ELISA (Fig. 1F). Using the purified antibodies, we confirmed one cross-reactive antibody C43, which had high binding affinity to hChi3l1 (K_D = 2 nM) (Fig. 1G) but somewhat lower binding affinity to mChi3l1 (K_D = 18 nM) (Fig. 1H).

The hChi3l1 and mChi3l1 protein sequences are conserved with 73.3% identity (Fig. 2A). To generate cross-reactive antibodies, we modified the immunization strategy by adding three additional boosts with mChi3l1 of Rabbit-#2 (Fig. 2B). After mChi3l1 boosting, the serum titer to mChi3l1 increased to the same level as to hChi3l1 (Fig. 2C). We then used mChi3l1 to bait the antigen-specific memory B cells. Of the 7 mChi3l1-positive single memory B cell cultures, 3 were cross-reactive (Fig. 2D). These antibodies were converted to rabbit IgG and their binding affinities to mChi3l1 and hChi3l1 were determined. All 7 antibodies exhibited high affinity binding to mChi3l1, with K_D values ranging from 1.4 to 5.6 nM (Fig. 2E–L). The 3 cross-reactive antibodies (C53, C56, and C59) also exhibited strong binding to hChi3l1, with K_D values ranging from 1.7 to 3.6 nM (Fig. 2E, G, H, and L).

Antibody C59 attenuates AILI *in vivo*

AILI involves both the direct hepatocyte damage and the inflammatory responses. Since *in vitro* tests cannot fully replicate the conditions that occur during liver injury, the Chi3l1 antibodies were evaluated for their efficacy in a mouse liver injury model *in vivo*. To reduce the number of antibodies to be tested *in vivo*, we grouped the 7 mChi3l1 antibodies into 4 epitope bins: Bin 1 (C53, C55, and C56), Bin 2 (C59), Bin 3 (C61 and C68), and Bin 4 (C64) (Fig. 3A and B). We selected one antibody from each epitope bin for *in vivo* testing (Bin 1, C55; Bin 2, C59; Bin 3, C61; and Bin 4, C64). The mice (3-6 mice/group) were treated by i.p. injection of 5 μg of the individual Chi3l1 antibodies 3 hours post-APAP challenge (Fig. 3C). Antibodies C59 and C55 significantly attenuated AILI, evident by the 10–200 folds reduction of serum ALT levels at 6 and 24 hours after APAP injection (Fig. 3D and E). Even though the efficacy is comparable between C55 and C59 in reducing ALT levels at 6 hours (Fig. 3D), C59 performed much better than C55 at 24 hours, with nearly 20-fold lower ALT levels (Fig. 3E). More importantly, while C55 is specific to mChi3l1 only, C59 is cross-reactive to both mChi3l1 and hChi3l1. Thus, we focused on C59 for further characterization.

The structure of C59 bound to hChi3l1

To delineate the molecular basis of Chi3l1 binding by C59, we determined the structure of the Chi3l1 + C59-Fab complex by X-ray crystallography at a resolution of 3.3 Å (PDB: 8DF1, Table 1). The asymmetric unit of this structure contained a total of six copies of Chi3l1, each bound by a single C59 Fab (Fig. 4). Chi3l1 presents an (α/β)8-barrel structure and has an *N*-linked glycan at Asn60 (Fig. 4A). The CDRs of both the heavy chain and light chain of C59 are involved in direct Chi3l1 interaction (Fig. 4A). Analysis of the binding interface revealed that HCDR1, HCDR3, LCDR1, and LCDR3 make direct contact with the 4α-5β loop and the 4α-helix of Chi3l1 (Fig. 4A). Specifically, Tyr34 in the HCDR1 interacts with Gln166 and Pro167 in the Chi3l1 4α-5β loop. Asn100 of HCDR3 contacts Arg128 in the 4α-helix of Chi3l1 (Fig. 4B). The C59 light chain CDRs also contribute extensively to the formation of the binding interface (Fig. 4C). The LCDR3 binds to the 4α-5β loop and the LCDR1 binds to the 4α-helix. The backbones of residues Tyr92 and Tyr94 in the LCDR3 form a series of hydrogen bonds with Chi3l1 residues in the 4α-5β loop (Gln166, Lys169) (Fig. 4C). Tyr92 of C59 inserts into the valley between the loop and 4α-helix, interacting with Lys169 and Arg128 from the loop and the helix,

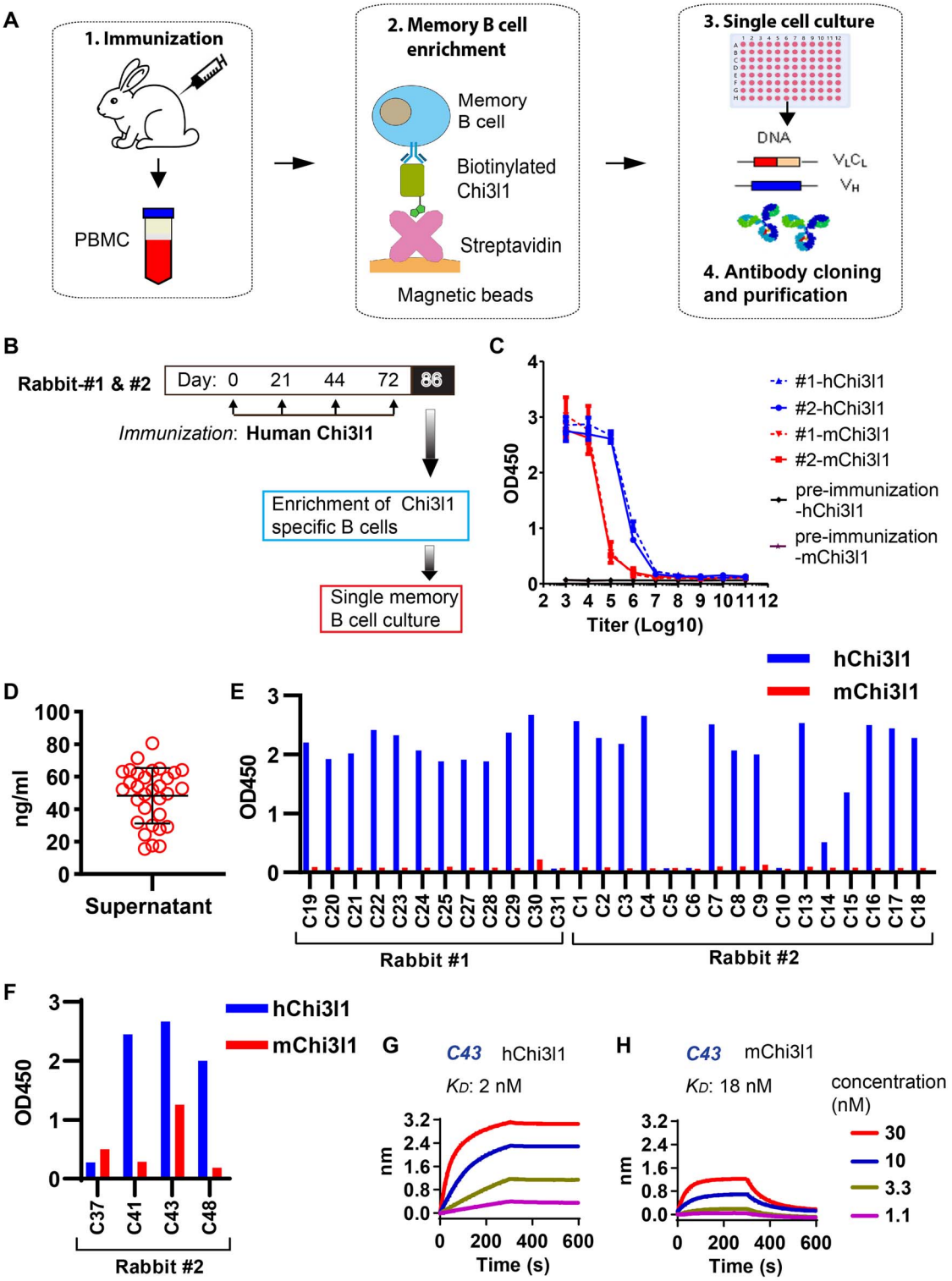

Figure 1. Generation and characterization of hChi3l1-blocking mAbs. (A) The flowchart of rabbit mAb generation. Two rabbits were immunized with Chi3l1 protein, and after 86 days, PBMCs were isolated. The antigen-specific memory B cells were then enriched by Streptavidin-Magnetic beads and biotinylated Chi3l1. Single memory B cells were cultured in 96-well plates with a density of one cell/per well. After 14 days, antibodies secreted by survived memory B cells were measured for antigen binding. The antibody genes were amplified from positive B cells. The antibodies were expressed and purified for functional assays. (B) The immunization strategy to generate anti-hChi3l1 antibody. Two rabbits (#1 and #2) were immunized with hChi3l1 on the indicated days. Two weeks after the final dose of injection on day 72, single memory B cells were isolated by hChi3l1 baiting, and cultured for 14 days. (C) The serum titer of immunized rabbits (#1 and #2) to hChi3l1 and mChi3l1 at day 86. The *X*-axis shows the dilution of the serum in the ELISA. (D) The average antibody concentration is 48.3 ng/mL in the supernatant of the single B cells. (E) The binding of the supernatant antibodies to hChi3l1 and mouse Chi3l1 (mChi3l1) was measured by ELISA. (F) The mChi3l1-specific single memory B cells were isolated at day 86 and cultured for two weeks. Binding of the four positive B cell supernatants to hChi3l1 and mChi3l1 was measured by ELISA. (G-H) The binding affinities of antibody C43 to hChi3l1 (G) and mChi3l1 (H) as determined by BLI-Octet.

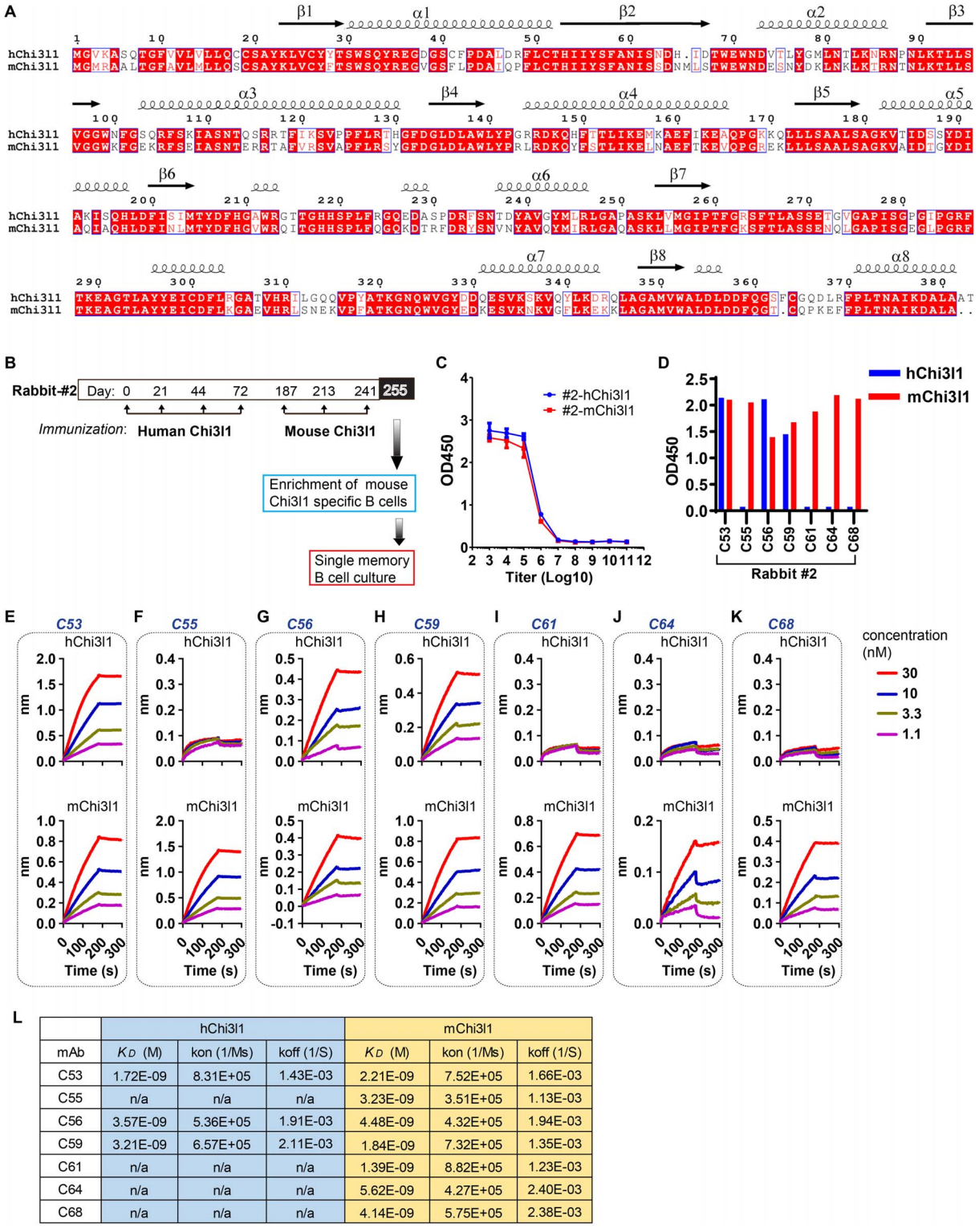

L

	hChi3l1			mChi3l1		
mAb	K_D (M)	kon (1/Ms)	koff (1/S)	K_D (M)	kon (1/Ms)	koff (1/S)
C53	1.72E-09	8.31E+05	1.43E-03	2.21E-09	7.52E+05	1.66E-03
C55	n/a	n/a	n/a	3.23E-09	3.51E+05	1.13E-03
C56	3.57E-09	5.36E+05	1.91E-03	4.48E-09	4.32E+05	1.94E-03
C59	3.21E-09	6.57E+05	2.11E-03	1.84E-09	7.32E+05	1.35E-03
C61	n/a	n/a	n/a	1.39E-09	8.82E+05	1.23E-03
C64	n/a	n/a	n/a	5.62E-09	4.27E+05	2.40E-03
C68	n/a	n/a	n/a	4.14E-09	5.75E+05	2.38E-03

Figure 2. Generation and characterization of cross-reactive mAbs. (A) The protein sequence alignment of human and mouse Chi3l1 was generated and analyzed using ClustalW2 (http://www.ebi.ac.uk/Tools/msa/clustalw2/) and ESPript 3.x (http://espript.ibcp.fr/ESPript/ESPript/). The UniProt accession numbers are P36222 (hChi3l1), Q61362 (mChi3l1), respectively. Identical residues are shown as white text on a red background, and similar residues are shown as red text. The secondary structure of Chi3l1 is displayed above the residue numbers. The β-strands and α-helix are labeled in the figure. (B) Rabbit-#2 was immunized with hChi3l1, followed by three mChi3l1 boosts on the indicated days. Two weeks after the final dose of injection on day 241, the memory B cells were isolated through mChi3l1 baiting and cultured. (C) The serum titer of immunized rabbit (#2) to hChi3l1 and mChi3l1 at day-255 after mChi3l1 boosting. The *X*-axis shows the dilution of the serum in the ELISA. (D) The binding of B cell supernatants (Rabbit-#2) to hChi3l1 and mChi3l1 was measured by ELISA. (E–K) The affinity of the antibodies that bind to hChi3l1 and mChi3l1. Three of the antibodies, C53, C56, and C59, are cross-reactive antibodies to both hChi3l1 and mChi3l1. (L) The affinity of anti-mChi3l1 and cross-reactive antibodies to hChi3l1 and mChi3l1 (n/a: not applicable). The equilibrium dissociation constant (K_D) was determined by the curve fitting analyses using the ForteBio's data analysis software.

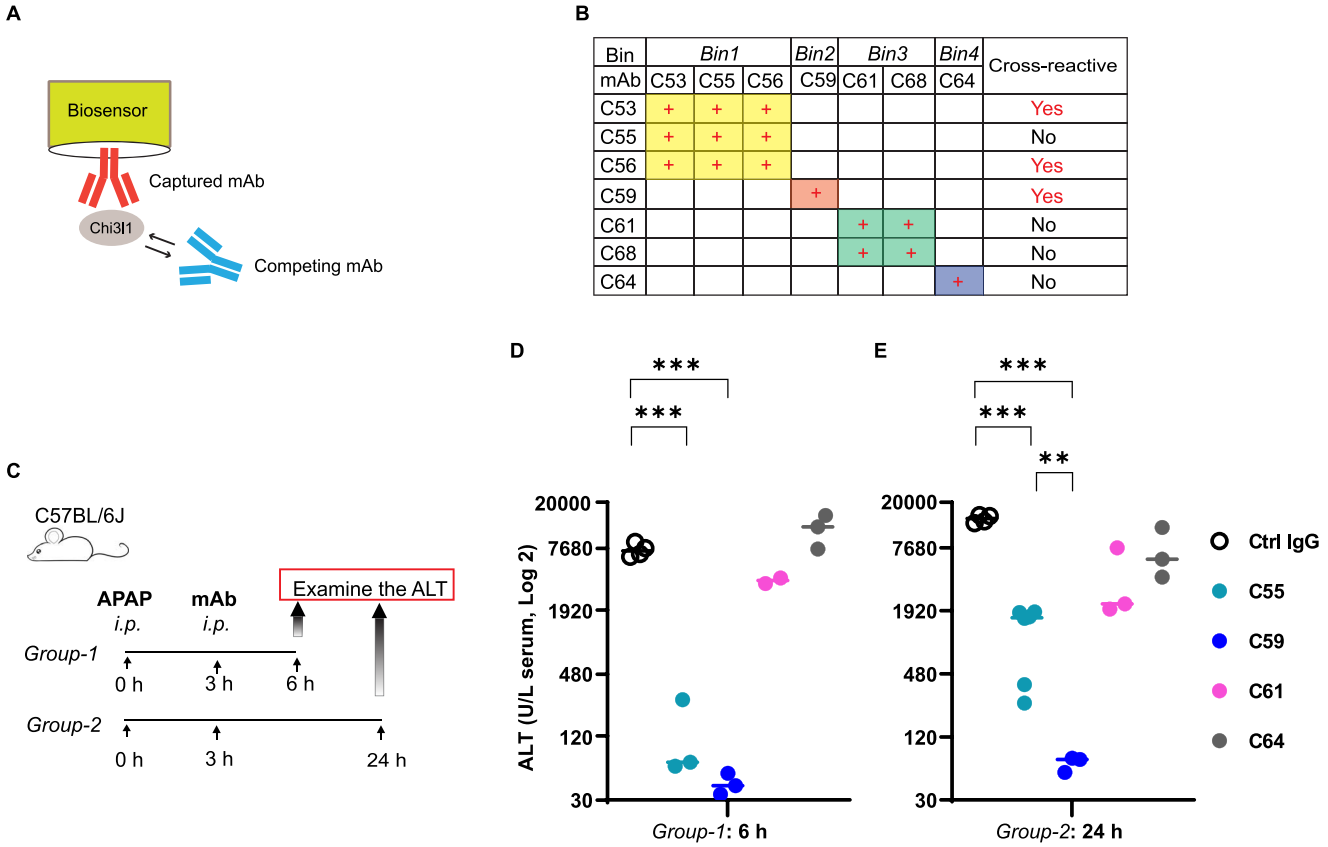

Bin	Bin1			Bin2	Bin3		Bin4	Cross-reactive
mAb	C53	C55	C56	C59	C61	C68	C64	
C53	+	+	+					Yes
C55	+	+	+					No
C56	+	+	+					Yes
C59				+				Yes
C61					+	+		No
C68					+	+		No
C64							+	No

Figure 3. Rabbit antibody C59 attenuates acute liver injury. (A) A cartoon representation of the sandwich epitope binning assay by Bio-Layer Interferometry. The first antibody was captured on the biosensor tip and binds to the Chi3l1. If the second antibody in the solution competes for the Chi3l1 binding with the first mAb, they bind to the overlapped epitope (same bin). (B) The anti-mouse Chi3l1 antibodies are divided into four bins (as indicated by different colors) based on the antibody binning assay. Antibodies grouped in the bin are labeled as "+". (C) The design of the *in vivo* antibody characterization. C57BL/6J mice (3-6 mice/group) were injected (i.p.) with APAP. After 3 hours, mice were treated (i.p.) with either a control IgG (Ctrl IgG) or the Chi3l1 antibodies (C55, C59, C61, and C64). (D and E) Serum alanine Transferase (ALT) concentrations were detected at 6 and 24 hours, respectively, after APAP challenge. *** indicates $p < 0.001$, ** indicates $p < 0.05$. A two-tailed, unpaired Student's *t*-test was performed.

respectively (Fig. 4C). The LCDR1 lays parallel to the 4α-helix, with Gln27 and Lys31 of C59 interacting with Lys121 and Thr129 in the Chi3l1 4α-helix (Fig. 4C). It is interesting to note that the side chain of Phe67 in the FR3 extends and contributes to the formation of the binding interface (Fig. 4C). The light chain of C59 contributes significantly to the interactions with Chi3l1 as compared to the heavy chain. The Arg128, Gln166, and Pro167 residues in the Chi3l1 epitope are conserved in both human and mouse Chi3l1. Other variant residues which form critical contacts (Lys121, Thr129, and Lys169) are relatively conserved (Arg121, Ser129, and Arg169) in the mouse homolog, providing a molecular basis for the cross-reactivity that C59 exhibits.

Humanized C59 antibody retains efficacy in attenuating AILI *in vivo*

To develop a potential antibody therapy for AILI, we humanized the rabbit antibody C59 by a modified CDR grafting strategy as reported previously [23, 25]. Briefly, the human germlines with the closest amino acid sequence identities to the C59 heavy- and light-chain variable regions were identified by IMGT/DomainGapAlign (Fig. 5A and B). The sequences that have the least number of polymorphisms were heavy-chain germline IGHV3–53 and light-chain germline IGKV1–39 (Fig. 5A and B). The CDRs of C59 determined by Kabat numbering were grafted into the human germline frameworks. Some critical residues adjacent to the CDRs (HCDR1, HCDR2, LCDR1, and LCDR2) were back-mutated to the original rabbit residues to preserve the binding affinity based on previous studies (Fig. 5A and B) [25, 26].

The affinities of humanized C59 (first version: hC59–1) to hChi3l1 and mChi3l1 were diminished by 5-fold (from 8 to 40 nM) and 100-fold (from 7 to 600 nM), respectively (Fig. 5C–F, and I). Based on the Chi3l1 + C59 complex structure, in which the C59 light chain contributes more to the antibody binding than the heavy chain, we focused on optimizing the C59 kappa chain to restore the binding of hC59 to both hChi3l1 and mChi3l1. As determined through our structural studies, there is an interaction between the light chain FR3 (Phe67) and hChi3l1. A single back mutation of S67F in the FR3 rescued the binding affinity of the humanized C59 (second version: hC59) to both hChi3l1 (K_D = 9 nM) and mChi3l1 (K_D = 7 nM) (Fig. 5G–I). However, the binding affinity cannot be

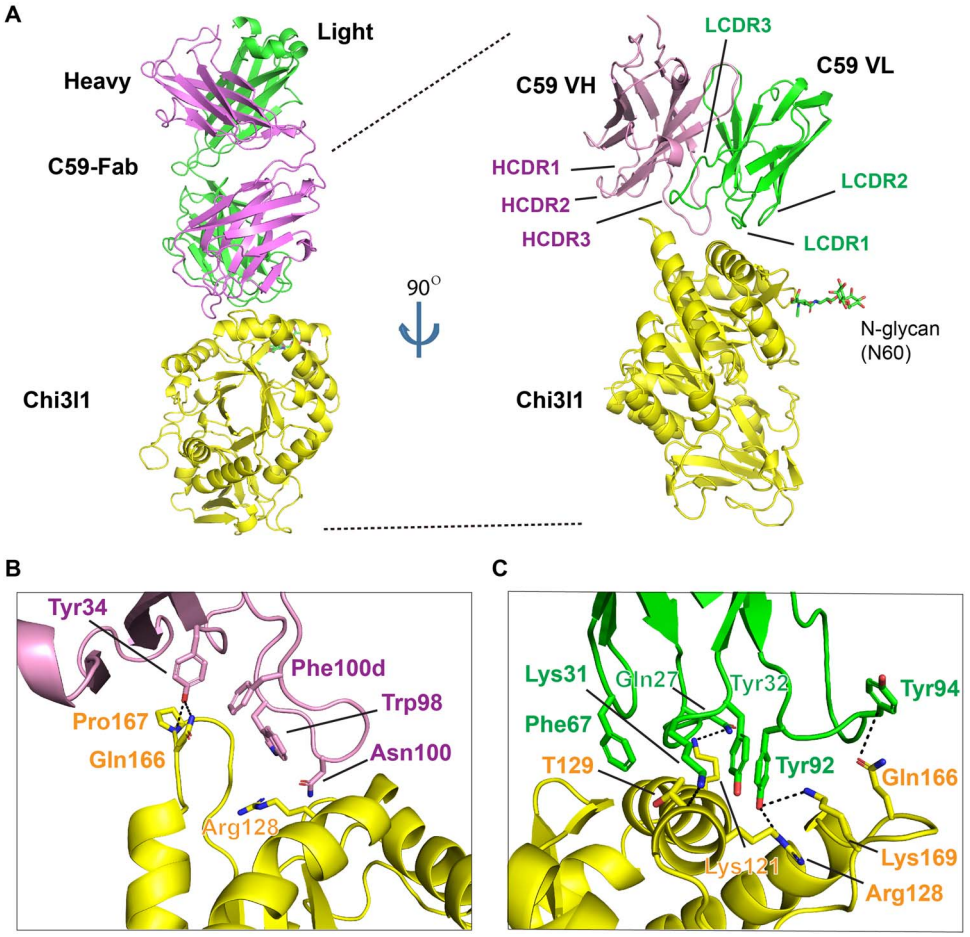

Figure 4. Crystal structure of the C59 + Chi3l1 complex. (A) The structure of hChi3l1 + C59 Fab complex (PDB: 8DF1). The hChi3l1 is colored yellow, the antibody C59 heavy (H) chain is shown in pink, and its light (L) chain in green. The C59 binding epitope is composed of the α4-β5 loop and α4-helix of Chi3l1. Chi3l1 has an *N*-linked glycan at the position Asn60 as indicated. (B) The interface between C59 VH and Chi3l1. Side chain-specific interactions are indicated by the dotted lines. (C) The interface between C59 VL and Chi3l1. Side chain-specific interactions are indicated by the dotted lines. Residues involved in the interaction are shown as sticks and labeled. The C59 residues are numbered according to Kabat numbering system.

rescued by the mutations of other amino acids in the FR3 (Fig. 5I and J).

To test the efficacy of the hC59 in attenuating AILI, we injected (i.p.) WT mice with both hC59 and the rabbit C59 (5 μg/mouse, 4-6 mice/group) 3 hours after the APAP challenge. Similar to the parental rabbit C59, the hC59 significantly attenuated AILI, as measured by the reduced serum ALT levels at 24 hours after the APAP injection when compared to the control antibody (Fig. 6A and B). The ALT level decreased by 7-fold after treatment with hC59 compared to the human antibody control. Moreover, compared with the rabbit C59, the hC59 is equally effective in attenuating liver necrosis (Fig. 6C–F). Together, these data indicate that the hC59 retains the *in vitro* and *in vivo* functions of the parental antibody and is a potential therapy to treat AILI.

DISCUSSION

APAP is one of the most commonly used drugs, but APAP overdose causes acute liver injury and systemic inflammatory responses, which can lead to liver failure [1]. NAC is the only antidote to treat APAP overdose-induced liver injury. However, the efficacy of NAC declines rapidly when used more than a few hours after APAP overdose [4]. Specific immune-modulatory therapies, which have the potential to inhibit the over-reactive inflammatory response and promote liver healing, are considered to be an optional treatment strategy [11, 32].

A recent study showed that heparan sulfate octadecasaccharide can dramatically attenuate the AILI in mice by neutralizing the proinflammatory activity of HMGB1, a key DAMP member that is correlated with the initiation of inflammation in liver injury [11]. Previous studies have also demonstrated that antibodies targeting the progress of inflammatory responses could attenuate AILIs [32, 33]. An antibody to HMGB1, significantly reduced the liver damage and intrahepatic inflammation during AILI [33]. In another study, inhibition of the platelet CLEC-2 signaling by a podoplanin-targeted antibody, which blocks the cross-talk between platelets and neutrophils, attenuated AILI in mice [32]. These studies demonstrated the feasibility of using immunotherapeutics in the treatment of AILI.

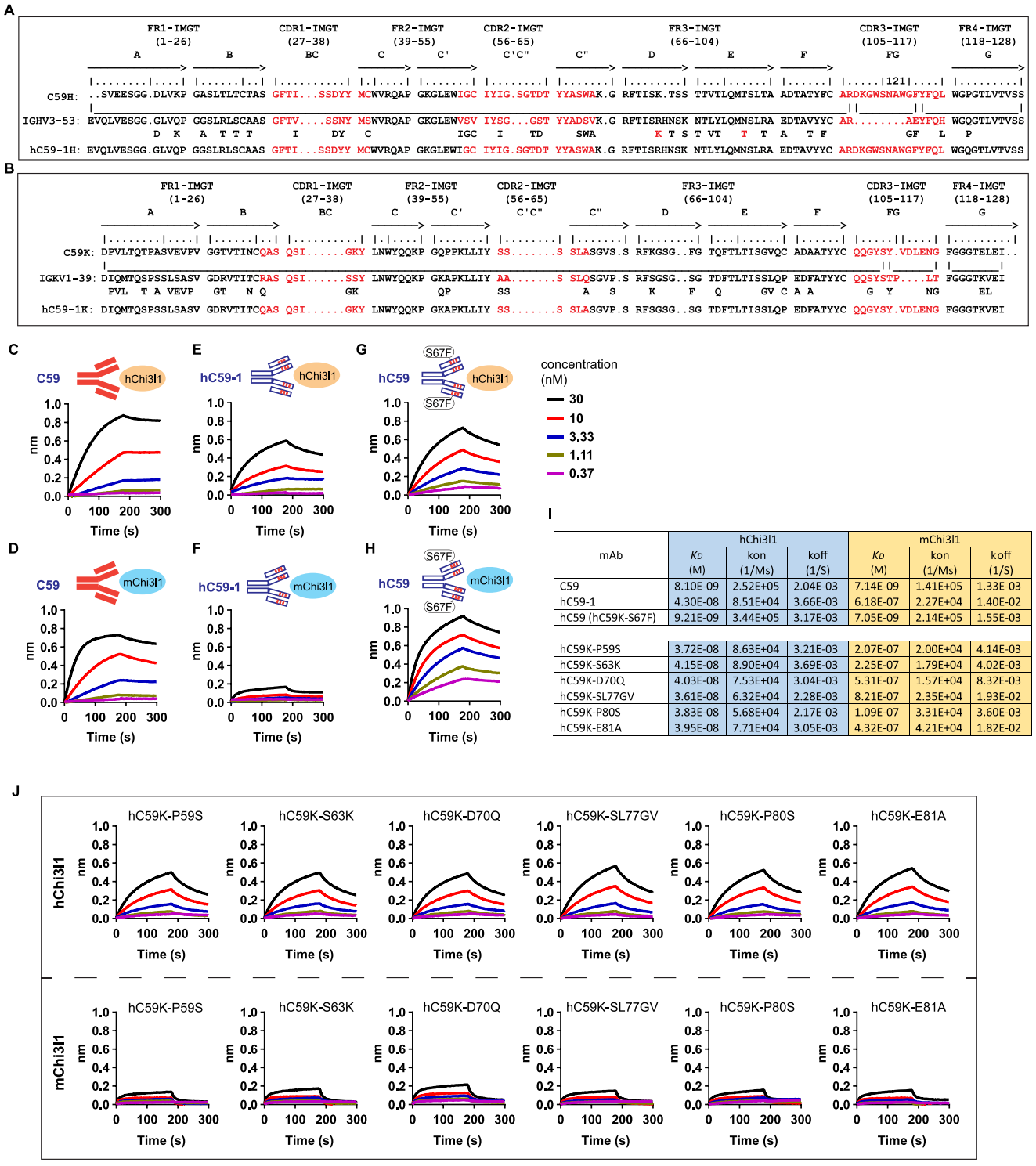

mAb	hChi3l1			mChi3l1		
	*K*D (M)	kon (1/Ms)	koff (1/S)	*K*D (M)	kon (1/Ms)	koff (1/S)
C59	8.10E-09	2.52E+05	2.04E-03	7.14E-09	1.41E+05	1.33E-03
hC59-1	4.30E-08	8.51E+04	3.66E-03	6.18E-07	2.27E+04	1.40E-02
hC59 (hC59K-S67F)	9.21E-09	3.44E+05	3.17E-03	7.05E-09	2.14E+05	1.55E-03
hC59K-P59S	3.72E-08	8.63E+04	3.21E-03	2.07E-07	2.00E+04	4.14E-03
hC59K-S63K	4.15E-08	8.90E+04	3.69E-03	2.25E-07	1.79E+04	4.02E-03
hC59K-D70Q	4.03E-08	7.53E+04	3.04E-03	5.31E-07	1.57E+04	8.32E-03
hC59K-SL77GV	3.61E-08	6.32E+04	2.28E-03	8.21E-07	2.35E+04	1.93E-02
hC59K-P80S	3.83E-08	5.68E+04	2.17E-03	1.09E-07	3.31E+04	3.60E-03
hC59K-E81A	3.95E-08	7.71E+04	3.05E-03	4.32E-07	4.21E+04	1.82E-02

Figure 5. Humanization of the rabbit C59 antibody. (A-B) The sequence alignment of rabbit C59, humanized C59 (first version, hC59–1), and the closest human antibody germline. (A) The hC59–1 heavy chain (hC59–1H), and (B) The hC59–1 kappa chain (hC59–1K). The CDR1–3 regions as defined by Kabat numbering are colored in red. The full amino acid sequences of the variable heavy (VH) and light (VL) chains are given using the standard one-letter code. (C-D) The binding curves of the rabbit C59 to hChi3l1 and mChi3l1. (E-F) The binding curves of the hC59–1 to hChi3l1 and mChi3l1. (G-H) The binding curves of hC59 (second version), which has an extra S67F reverse mutation in the kappa chain FR3 region of hC59–1. The binding affinity of hC59 was rescued by the single mutation. (I) The equilibrium dissociation constant (K_D) and the kinetic rate constants (kon, koff) were determined from the curve fitting analyses of antibody-Chi3l1 binding result. (J) The binding curves of humanized C59 with the reversed mutations in the FR3 region of the kappa chain. The antibody affinity was measured by OCTET RED96 (ForteBio).

Table 1. X-ray data collection and refinement statistics of Chi3l1-C59Fab

	Chi3l1 + C59 Fab
Data collection	
Facility	ALS 5.0.1
Wavelength (Å)	0.97
Space group	$P2_12_12_1$
Cell dimensions	
a, b, c (Å)	102.1, 172.9, 404.5
α, β, γ (°)	90.0, 90.0, 90.0
Resolution range (Å)	73.27–3.30 (3.42–3.30)
R_{merge}	0.796 (1.707)
CC1/2	0.265 (0.421)
I/σI	8.97 (1.87)
Completeness (%)	99.9 (99.8)
Redundancy	11.8 (11.7)
Refinement	
No. reflections	108,485 (10,685)
R_{work}/R_{free} (%)	20.2/24.0
No. non-hydrogen atoms	
Protein	36,612
Ligand/ion	278
B-factors (Å^2)	
Protein	70.9
Ligand	102.8
Wilson B-factor (Å^2)	56.9
R.m.s. deviations	
Bond lengths (Å)	0.007
Bond angles (°)	0.96
Ramachandran (%)	
Favored	96.7
Allowed	3.1
Outliers	0.2
PDB ID	8DF1

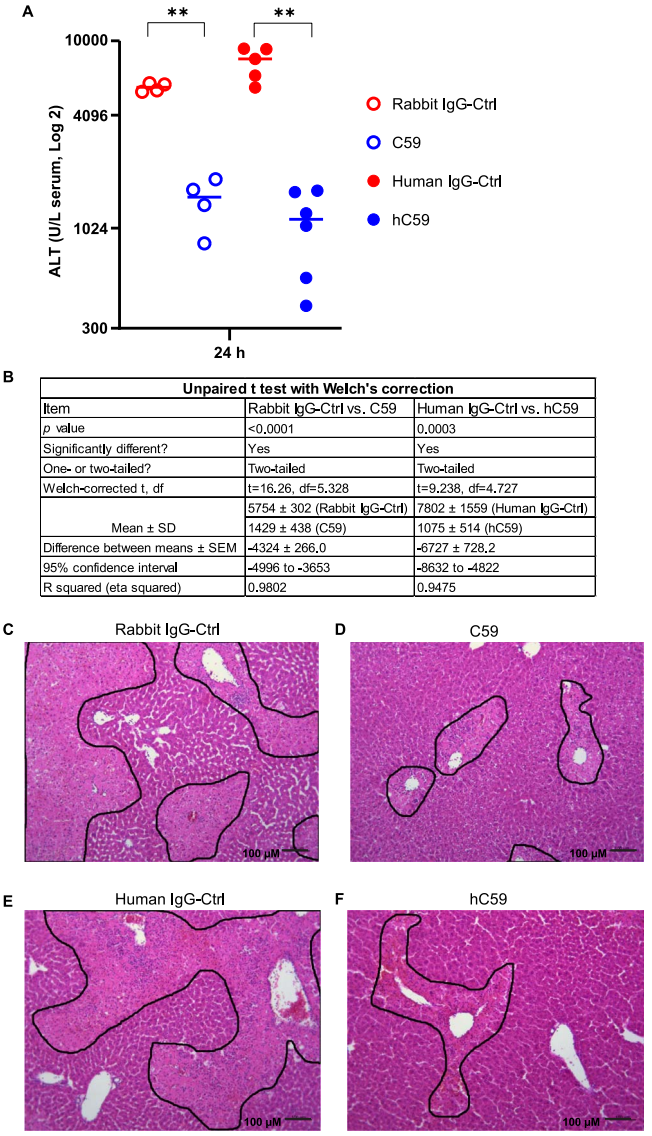

Figure 6. The hC59 attenuates acute liver injury. (A) C57BL/6J mice (4–6 mice/group) were injected (i.p.) with APAP. After 3 hours, the mice were treated (i.p.) with a rabbit IgG-control (Ctrl), the original rabbit antibody C59, a human IgG-Ctrl, or the humanized C59 (hC59). Serum ALT concentrations were measured at 24 hours after APAP injection. A two-tailed, unpaired Student's *t*-test was performed. ** indicates $p < 0.001$. (B) The results table of unpaired t test with Welch's correction. (C–F) Liver histology was evaluated at 24 hours after APAP injection. Injured areas are outlined. (C) Rabbit IgG-Ctrl, (D) Rabbit C59, (E) Human IgG-Ctrl, (F) hC59, and scale bar, 100 μm. (4-6 mice/group).

We reported previously that Chi3l1 is expressed in the liver of patients with APAP-induced liver failure, but we could not detect Chi3l1 in biopsies of healthy livers. Similarly, in the mouse model of AILI, we observed a rapid and marked overexpression of Chi3l1 after APAP challenge [12]. In Chi3l1 knockout mice, we found that the APAP-induced liver injury level was markedly reduced [12]. Thus, disruption of Chi3l1 could be a novel therapy for AILI. In this study, we selected a rabbit mAb to Chi3l1, evaluated the efficacy of the antibody *in vivo*, defined its functional epitope, and humanized the rabbit antibody for further drug development. Due to the higher diversity and sensitivity of rabbit antibodies to various antigens [34, 35], rabbit antibodies have been broadly used as diagnostic and research tools [36]. More recently, multiple humanized mAbs originated from rabbit have been approved for clinical use or are being tested in clinical trials [37, 38]. In 2019, the first humanized rabbit antibody (brolucizumab) that inhibits VEGF for the treatment of age-related macular degeneration, was approved by the FDA [39]. Cloning of mAbs from single B cells of immunized animals or humans infected with pathogens has been well developed as a source of therapeutic antibodies [40]. These include single plasma cell sorting, single memory B cell culture, and a combination of single B cell sorting with phage library construction [41].

By modifying and optimizing reported single memory B cell culture protocols [42, 43], we developed a strategy of successive immunization with hChi3l1 and mChi3l1, coupled with antigen-specific memory B cell sorting to isolate cross-reactive mAbs from the single memory B cells of immunized rabbits. The successive immunizations with hChi3l1 and mChi3l1 induced the cross-reactive

antibodies with higher binding affinity to both hChi3l1 and mChi3l1. After immunization, we enriched the antigen-specific memory B cells for culturing. The Avitag in our monomeric hChi3l1 and mChi3l1 antigens ensures only one site-specific biotinylation to the antigen without masking potential epitopes and increases the success rate of antigen baiting. In the memory B cell culture system, we used the mouse EL4-B5 feeder cell, combined with rabbit IL-2 and IL-21, to support the differentiation and survival of the memory B cells based on a previous study [42]. Once the single memory B cells are cultured, the paired antibody genes encoding the heavy and light chain variable regions can be isolated and converted to IgGs for further characterization. This platform significantly advances the generation of rabbit mAbs for drug development.

While the cross-reactive antibody C59 attenuates the liver injury *in vivo*, other antibodies with high Chi3l1 binding affinity did not show any efficacy in the same animal model. This finding suggests that not only the binding affinity but also the specific epitope of Chi3l1-directed antibodies is critical to its efficacy *in vivo*. Based on the structure of Chi3l1 + C59 complex, C59 binds to the 4α-5β loop and 4α-helix of hChi3l1. The C59 binding is largely contributed by the light chain, which deviates from previous studies in which both heavy chain and light chain of rabbit antibody are critical for the antigen-binding [25, 44]. Nevertheless, the light chain dominance in rabbit antibody paratopes has been reported in a previous study [45]. On the other hand, the diversity of rabbit antibody generated by heavy chain rearrangement is limited, as only one germline VH1 is predominantly used. However, rabbit kappa chain contributes more to the diversity of antibody repertoire than that of human and mouse antibodies [46]. Rabbits have two kappa chain isotypes, K1 and K2, which compensate for the limited diversity at heavy chain locus. It also suggests that rabbit antibody kappa chain may contribute more to the paratopes of the antibody.

Humanization of C59 is an essential step to reduce the risk of immunogenicity after repeated administration in clinical applications [47]. The CDR grafting generated the first version of humanized C59 (hC59–1). However, this initial strategy resulted in a dramatic reduction in binding affinity. Based on the C59 + Chi3l1 structure, the light chain CDR3 contained the majority portion of hydrogen bonds interaction with Chi3l1, and FR3 of kappa chain also interacts with the Chi3l1. We introduced single mutations to the kappa-FR3, and one of the backing mutations S67F rescued the binding affinity of hC59 to both hChi3l1 and mChi3l1 and retained the *in vivo* properties of the parental antibody in AILI model. In addition to liver injury, Chi3l1 has been implicated in a variety of other diseases, including cancer, arthritis, and Alzheimer's disease [48]. Identification of the 4α-5β loop and 4α-helix as a major hotspot for blocking antibodies will facilitate the isolation of Chi3l1 blocking antibodies as potential therapies for liver injuries and other human diseases.

SUPPLEMENTARY DATA

Supplementary Data are available at ABT Online.

AVAILABILITY OF DATA AND MATERIALS

The datasets used and/or analyzed during the current study are available from the corresponding authors on reasonable request.

ACKNOWLEDGEMENTS

We thank Dr. Xunjun Fan for her assistance in the animal experiments.

AUTHORS' CONTRIBUTIONS

Conceptualization was by L.L., D.W., J.S.M., N.Z., C.J., and Z.A.; methodology was by L.L., Y.W., D.W., J.J., P.Z., W.X., C.L.A., Z.S., D.H., and N.Z.; writing—original draft preparation was by L.L., D.W., and Z.A.; writing—review and editing was by L.L., D.W., P.Z., J.S.M., and Z.A.; supervision was by J.S.M., N.Z., C.J., and Z.A.; project administration was by J.S.M., N.Z., C.J., and Z.A.; funding acquisition was by C.J. and Z.A. All authors read and approved the final manuscript.

ANIMAL RESEARCH

The rabbit and mouse experiments were approved by the Animal Welfare Committee of the University of Texas Health Science Center at Houston and were conducted following the US Public Health Service Policy on Humane Care and Use of Laboratory Animals.

FUNDING

This study was funded in part by the NIH (RO1 Grant no. DK122708 to C.J.), the Cancer Prevention and Research Institute of Texas (Grants no. RP150551 and RP190561 to Z.A.), and Welch Foundation (Grant no. AU-0042-20030616 to Z.A.).

CONFLICT OF INTEREST STATEMENT

The University of Texas System has filed a patent application on the Chi3l1 targeting antibodies, and C.J., J.J., Z.S., L.L., N.Z., and Z.A. are named as the inventors of the patent application. Z.A. holds the position of deputy editor-in-chief of Antibody Therapeutics and is blinded from reviewing or making decisions for the manuscript.

ETHICS AND CONSENT STATEMENT

Not applicable.

REFERENCES

1. Bernal, W, Wendon, J. Acute liver failure. *N Engl J Med* 2013; **369**: 2525–34.
2. Blieden, M, Paramore, LC, Shah, D *et al.* A perspective on the epidemiology of acetaminophen exposure and toxicity in the United States. *Expert Rev Clin Pharmacol* 2014; **7**: 341–8.
3. Lee, WM. Acetaminophen toxicity: changing perceptions on a social/medical issue. *Hepatology* 2007; **46**: 966–70.

4. Larson, AM, Polson, J, Fontana, RJ *et al.* Acetaminophen-induced acute liver failure: results of a United States multicenter, prospective study. *Hepatology* 2005; **42**: 1364–72.
5. Mitchell, JR, Jollow, DJ, Potter, WZ *et al.* Acetaminophen-induced hepatic necrosis. I. Role of drug metabolism. *J Pharmacol Exp Ther* 1973; **187**: 185–94.
6. Mossanen, JC, Tacke, F. Acetaminophen-induced acute liver injury in mice. *Lab Anim* 2015; **49**: 30–6.
7. Brenner, C, Galluzzi, L, Kepp, O *et al.* Decoding cell death signals in liver inflammation. *J Hepatol* 2013; **59**: 583–94.
8. James, LP, Simpson, PM, Farrar, HC *et al.* Cytokines and toxicity in acetaminophen overdose. *J Clin Pharmacol* 2005; **45**: 1165–71.
9. Bianchi, ME, Crippa, MP, Manfredi, AA *et al.* High-mobility group box 1 protein orchestrates responses to tissue damage via inflammation, innate and adaptive immunity, and tissue repair. *Immunol Rev* 2017; **280**: 74–82.
10. Huebener, P, Pradere, JP, Hernandez, C *et al.* The HMGB1/RAGE axis triggers neutrophil-mediated injury amplification following necrosis. *J Clin Invest* 2015; **125**: 539–50.
11. Arnold, K, Xu, Y, Sparkenbaugh, EM *et al.* Design of anti-inflammatory heparan sulfate to protect against acetaminophen-induced acute liver failure. *Sci Transl Med* 2020; **12**: eavv8075.
12. Shan, Z, Li, L, Atkins, CL *et al.* Chitinase 3-like-1 contributes to acetaminophen-induced liver injury by promoting hepatic platelet recruitment. *elife* 2021; **10**: e68571.
13. Kzhyshkowska, J, Gratchev, A, Goerdt, S. Human chitinases and chitinase-like proteins as indicators for inflammation and cancer. *Biomark Insights* 2007; **2**: 117727190700200023.
14. Donnelly, LE, Barnes, PJ. Acidic mammalian chitinase–a potential target for asthma therapy. *Trends Pharmacol Sci* 2004; **25**: 509–11.
15. Renkema, GH, Boot, RG, Strijland, A *et al.* Synthesis, sorting, and processing into distinct isoforms of human macrophage chitotriosidase. *Eur J Biochem* 1997; **244**: 279–85.
16. Kzhyshkowska, J, Yin, S, Liu, T *et al.* Role of chitinase-like proteins in cancer. *Biol Chem* 2016; **397**: 231–47.
17. Knorr, T, Obermayr, F, Bartnik, E *et al.* YKL-39 (chitinase 3-like protein 2), but not YKL-40 (chitinase 3-like protein 1), is up regulated in osteoarthritic chondrocytes. *Ann Rheum Dis* 2003; **62**: 995–8.
18. Mohanty, AK, Fisher, AJ, Yu, Z *et al.* Cloning, expression, characterization and crystallization of BRP39, a signalling glycoprotein expressed during mammary gland apoptosis. *Protein Expr Purif* 2009; **64**: 213–8.
19. Ngernyuang, N, Yan, W, Schwartz, LM *et al.* A heparin binding motif rich in arginine and lysine is the functional domain of YKL-40. *Neoplasia* 2018; **20**: 182–92.
20. Mohanty, AK, Singh, G, Paramasivam, M *et al.* Crystal structure of a novel regulatory 40-kDa mammary gland protein (MGP-40) secreted during involution. *J Biol Chem* 2003; **278**: 14451–60.
21. Lee, CG, Hartl, D, Lee, GR *et al.* Role of breast regression protein 39 (BRP-39)/chitinase 3-like-1 in Th2 and IL-13–induced tissue responses and apoptosis. *J Exp Med* 2009; **206**: 1149–66.
22. Li, L, Freed, DC, Liu, Y *et al.* A conditionally replication-defective cytomegalovirus vaccine elicits potent and diverse functional monoclonal antibodies in a phase I clinical trial. *NPJ Vaccines* 2021; **6**: 1–14.
23. Gui, X, Deng, M, Song, H *et al.* Disrupting LILRB4/APOE interaction by an efficacious humanized antibody reverses T-cell suppression and blocks AML development. *Cancer Immunol Res* 2019; **7**: 1244–57.
24. Li, L, Meng, W, Horton, M *et al.* Potent neutralizing antibodies elicited by dengue vaccine in rhesus macaque target diverse epitopes. *PLoS Pathog* 2019; **15**: e1007716.
25. Yu, Y, Lee, P, Ke, Y *et al.* A humanized anti-VEGF rabbit monoclonal antibody inhibits angiogenesis and blocks tumor growth in xenograft models. *PLoS ONE* 2010; **5**: e9072.
26. Zhang, YF, Ho, M. Humanization of rabbit monoclonal antibodies via grafting combined Kabat/IMGT/Paratome complementarity-determining regions: Rationale and examples. *MAbs* 2017; Taylor & Francis, Vol. **9**: 419–29.
27. Evans, PR, Murshudov, GN. How good are my data and what is the resolution? *Acta Crystallogr D Biol Crystallogr* 2013; **69**: 1204–14.
28. Battye, TG, Kontogiannis, L, Johnson, O *et al.* iMOSFLM: a new graphical interface for diffraction-image processing with MOSFLM. *Acta Crystallogr D Biol Crystallogr* 2011; **67**: 271–81.
29. Emsley, P, Cowtan, K. Coot: model-building tools for molecular graphics. *Acta Crystallogr D Biol Crystallogr* 2004; **60**: 2126–32.
30. Adams, PD, Afonine, PV, Bunkoczi, G *et al.* PHENIX: a comprehensive Python-based system for macromolecular structure solution. *Acta Crystallogr D Biol Crystallogr* 2010; **66**: 213–21.
31. Croll, TI. ISOLDE: a physically realistic environment for model building into low-resolution electron-density maps. *Acta Crystallogr D Biol Crystallogr* 2018; **74**: 519–30.
32. Chauhan, A, Sheriff, L, Hussain, MT *et al.* The platelet receptor CLEC-2 blocks neutrophil mediated hepatic recovery in acetaminophen induced acute liver failure. *Nat Commun* 2020; **11**: 1939.
33. Lundbäck, P, Lea, JD, Sowinska, A *et al.* A novel high mobility group box 1 neutralizing chimeric antibody attenuates drug-induced liver injury and postinjury inflammation in mice. *Hepatology* 2016; **64**: 1699–710.
34. Hoang, LL, Tang, P, Hicks, DG *et al.* A new rabbit monoclonal E-cadherin antibody [EP700Y] shows higher sensitivity than mouse monoclonal E-cadherin [HECD-1] antibody in breast ductal carcinomas and does not stain breast lobular carcinomas. *Appl Immunohistochem Mol Morphol* 2014; **22**: 606–12.
35. Rocha, R, Nunes, C, Rocha, G *et al.* Rabbit monoclonal antibodies show higher sensitivity than mouse monoclonals for estrogen and progesterone receptor evaluation in breast cancer by immunohistochemistry. *Pathol Res Pract* 2008; **204**: 655–62.
36. Chauhan, A, Siegel, L, Freese, R *et al.* Performance of Ventana SP263 PD-L1 assay in endobronchial ultrasound guided-fine-needle aspiration derived non-small-cell lung carcinoma samples. *Diagn Cytopathol* 2021; **49**: 355–62.
37. O'Hara, MH, O'Reilly, EM, Varadhachary, G *et al.* CD40 agonistic monoclonal antibody APX005M (sotigalimab) and chemotherapy, with or without nivolumab, for the treatment of metastatic pancreatic adenocarcinoma: an open-label, multicentre, phase 1b study. *Lancet Oncol* 2021; **22**: 118–31.
38. Doberer, K, Duerr, M, Halloran, PF *et al.* A randomized clinical trial of anti-IL-6 antibody clazakizumab in late antibody-mediated kidney transplant rejection. *J Am Soc Nephrol* 2021; **32**: 708–22.
39. Sharma, A, Kumar, N, Kuppermann, BD *et al.* Brolucizimab—leading an era of structural revolution for long-term VEGF suppression. *Eye* 2020; **34**: 611–3.
40. Pedrioli, A, Oxenius, A. Single B cell technologies for monoclonal antibody discovery. *Trends Immunol* 2021; **42**: 1143–58.
41. Rashidian, J, Lloyd, J. Single B cell cloning and production of rabbit monoclonal antibodies. *Methods Mol Biol* 2020; **2070**: 423–41.
42. Weitkamp, JH, Kallewaard, N, Kusuhara, K *et al.* Generation of recombinant human monoclonal antibodies to rotavirus from single antigen-specific B cells selected with fluorescent virus-like particles. *J Immunol Methods* 2003; **275**: 223–37.
43. Seeber, S, Ros, F, Thorey, I *et al.* A robust high throughput platform to generate functional recombinant monoclonal antibodies using rabbit B cells from peripheral blood. *PLoS ONE* 2014; **9**: e86184.
44. Pan, R, Sampson, JM, Chen, Y *et al.* Rabbit anti-HIV-1 monoclonal antibodies raised by immunization can mimic the antigen-binding modes of antibodies derived from HIV-1-infected humans. *J Virol* 2013; **87**: 10221–31.
45. Goydel, RS, Weber, J, Peng, H *et al.* Affinity maturation, humanization, and co-crystallization of a rabbit anti-human ROR2 monoclonal antibody for therapeutic applications. *J Biol Chem* 2020; **295**: 5995–6006.
46. Sehgal, D, Johnson, G, Wu, TT *et al.* Generation of the primary antibody repertoire in rabbits: expression of a diverse set of Igk-V genes may compensate for limited combinatorial diversity at the heavy chain locus. *Immunogenetics* 1999; **50**: 31–42.
47. Davda, J, Declerck, P, Hu-Lieskovan, S *et al.* Immunogenicity of immunomodulatory, antibody-based, oncology therapeutics. *J Immunother Cancer* 2019; **7**: 1–9.
48. Zhao, T, Su, Z, Li, Y *et al.* Chitinase-3 like-protein-1 function and its role in diseases. *Signal Transduct Target Ther* 2020; **5**: 201.